The effects of annealing temperature on physical properties of $Ce_2Zr_2O_7$ material.

Yissah Saheed O.[1], Moise B Tchoula Tchokonte[2], Sibusiso Nqayi[1] and Buyisiwe Sondezi [1]

[1] Rare-Earth Based Oxides and Nano Materials Group, Department of Physics, University of Johannesburg Cnr. Kingsway Avenue and University Road, Ackland Park 2006, South Africa.
[2] Department of Physics and Astronomy, University of Western Cape, Private Bag X17, Bellville 7535, South Africa

E-mail: 224099692@student.uj.ac.za

Abstract. Pyrochlore oxides are a fascinating class of materials known for their remarkable thermal stability and adaptability, making them excellent candidates for energy-related applications. This study explored the effects of thermal treatment on structural, morphological, optical, thermodynamic and magnetic properties of $Ce_2Zr_2O_7$ nanoparticles (CZONPs) prepared using sol-gel method. Followed by thermal annealing treatment. The micro-structure, size, optical, and magnetic properties of prepared materials were analysed using X-ray diffraction (XRD), transmission electron microscopy (TEM), UV-Vis. photoluminescence spectroscopy, and physical properties measurement system (PPMS), respectively. The results showed mixed phases of $CeZrO_4$ and $Ce_2Zr_2O_7$ at various annealing temperature ranges. The ratio between these phases was changing as a function of annealing temperature. The pure phase of CZONPs was obtained at high temperature. These findings point to a strong correlation between pyrochlore's stability, making the material highly relevant for high-temperature applications.

1. Introduction

Pyrochlores are complex metal oxides with a general formula of $A_2B_2O_7$. Where A site represents an 8-fold coordinated metal, usually rare earth, and B site represents 6-fold coordinated metals such as transitional metals. The *A* site cation generally has an oxidation state of +2 or +3, and the *B* site cation has a corresponding oxidation state of +5 or +4 [1-2]. A study by (Fuentes et al., 20024) shows that the stable crystalline phase structure of an $A_2B_2O_7$ compound is determined ratio of the radius rA/rB [3]. When the radius ratio is greater than 1.78, a monoclinic layered perovskite phase will be observed. i.e. $P2_1$. When the radius ratio is the range of 1.46 -1.78 and ordered pyrochlore phase will be formed which belong to the space group (SG) of *Fd-3m*. This can also be referred to an ordered defective fluorite in which 1/8 of the oxygen are unoccupied [5-6]. If the radius ratio is within the range of 1.17 - 1.45 a disordered defective fluorite will be formed, which belong to the SG of Fm-3m. [3]. And if the radius ratio is close to 1.17 – 1.0 rare earth C-type phase will be formed. The structure is similar to Y_2O_3 whose A and B cation distribute even more randomly in the sublattices [3-4]. Previous studies have showed that X-ray diffraction (XRD) and transmission electron microscopy (TEM) spectroscopy are very effective in distinguishing $A_2B_2O_7$ compounds containing different phase structures [3].

Pyrochlore-type Cerium–zirconium oxide $Ce_2Zr_2O_7$ are attractive materials used as structural ceramic which have gained significant attention in recent years, due to its defect-tolerant structure, high oxygen mobility, and their ability to reversibly store and release oxygen, making them indispensable in automotive catalysts (AC), solid oxide fuel cells (SOFCs), and thermal barrier coatings (TBC) [2,3,4].

Synthesis methods greatly influence the final properties of Cerium–zirconium oxide with annealing temperature playing a pivotal role in defining phase composition and structural integrity [3,4,5,6]. Lower temperatures favours high surface areas and defect-rich structures, beneficial for catalysis, while higher temperatures improve crystallinity and thermal robustness [7]. Despite its importance, systematic studies on the effects of annealing on Cerium–zirconium oxide remain scarce. This research work aims to synthesis CZONPs and provides a detailed investigation of how annealing temperature modulates its structural, morphology, optical, thermodynamic, and magnetic, physical properties [6,8].

2. Experimental Procedure

2.1 Chemicals used

Cerium (II) nitrate hexahydrate, $Ce(NO_3)_3.6H_2O$ (with the assay of 99%, Sigma Aldrich) which has mass of 434.22g, and Zirconium (IV) sulphate hydrate, $Zr(SO_4)_2.4H_2O$ (with the assay of 99%, Sigma Aldrich) which has mass of 283.34g, and Citric Acid Anhydrous $C_6H_6O_7$ which has mass of 192.13g, ammonia (NH3) and Distilled water were used for the preparation of the materials.

2.2 Preparation procedure and synthesis of $Ce_2Zr_2O_7$ nanocomposite.

Nanocrystalline $Ce_2Zr_2O_7$ (CZONP) powder was produced using sol-gel method. To produce the powder the following compounds was used: above chemicals were uses. The molecular mass of $Ce_2Zr_2O_7$ was calculated after the determination of the stoichiometry, to produce 3 g of $Ce_2Zr_2O_7$ powder by sol-gel method, 4.34g of Ce $(NO_3)_3.6H_2O$ 2.83g of Zr $(SO_4)_2.4H_2O$ and 16.01g of $C_6H_6O_7$ were poured into a beaker with a magnetic stirrer, and 150ml of distilled water. The beaker was placed on a magnetic stirrer, and it was allowed to stir for 30 minutes before adding 3 drops of Ammonia (NH3) and it was allowed to stir for 1 hour 30 minutes, then allowed to age for 24 hours at room temperature. After aging, the sample forms gel and the beaker was placed on hot plate with temperate of 60^0C for 4hours 20mins for the gel to turn to dry. The materials were allowed to cool; it was crushed into fine powered using mortar and pestle and was divided into five (5) portions. The materials were then annealed at 500^0C, 800^0C, 1000^0C, 1200^0C and 1500^0C respectively at 4^0C/minute for four (4) hours in the air furnace.

The material was crushed again and ready for X-ray diffraction, XRD characterization. The Rietveld refinement of XRD patterns was carried out by using the material analysis using diffraction (MAUD) program.

2.3 Materials characterization

The annealed powdered materials were removed from the furnace and crushed, and the powder X-ray diffraction (PXRD) was performed using EMPYREAN X-RAY Diffractometer, Paralytical, Germany, with Ni-filtered Cu Kα radiation wavelength of 1.5406Å, working at 40 kV and 40 mA with the radiation with 2.5 step, (θ/2θ Bragg Brentano geometry). The PXRD measurements were performed in the 2θ range from 10° to 80°. Identification of present phases was conducted using MAUD v. 2.99 software [9].

The Rietveld structural refinement calculations were conducted using the obtained XRD data and the MAUD software to determine relevant structural parameters of the powders annealed at different temperatures.

Morphology and elemental distribution of the obtained annealed powders materials were analysed using a transmission electron microscopy (TEM), and scanning electron microscope (SEM) VEGA3, TESCAN, Czech Republic, operated at 20keV and coupled with X-max energy dispersive spectrometer (EDS).

3. Results and discussions

3.1 Structural analysis

The XRD patterns presented in Figure 1 indicate that the powder annealed at 500°C shows typical amorphous behaviour without a long range of atom ordering. Results indicate powder annealed at 800°C, 1000°C, 1200°C, and 1400°C shows a clear reflection peak with double phases of $Ce_2Zr_2O_8$ and ZrO_2, a diffraction peak at scattering angle (2θ) of 29°, 33°, 48°, 57°, and 60°, correspond to the reflections from (222), (400), (440), (622), and (444), crystal planes respectively as demonstrated in Figure 1(a). These reflections correspond to the Cubic $Ce_2Zr_2O_7$ structure as confirmed by the International Centre for Diffraction Data (ICDD) card number No. 04-002-0615 [16] which was detected at 1500°C suggesting the sample exhibits pure Pyrochlore phase in space group 227 (*Fd-3m*) [3] as shown in Figure 1 (b) as there was a peak shifted towards higher 2θ angle in Figure 1(b) as very narrow diffraction lines in its XRD pattern. This can further suggest its highly crystallinity state. The result of the structural Rietveld refinement of the XRD Pattern of $Ce_2Zr_2O_7$ annealed at 1500C is presented in Figure 2 below.

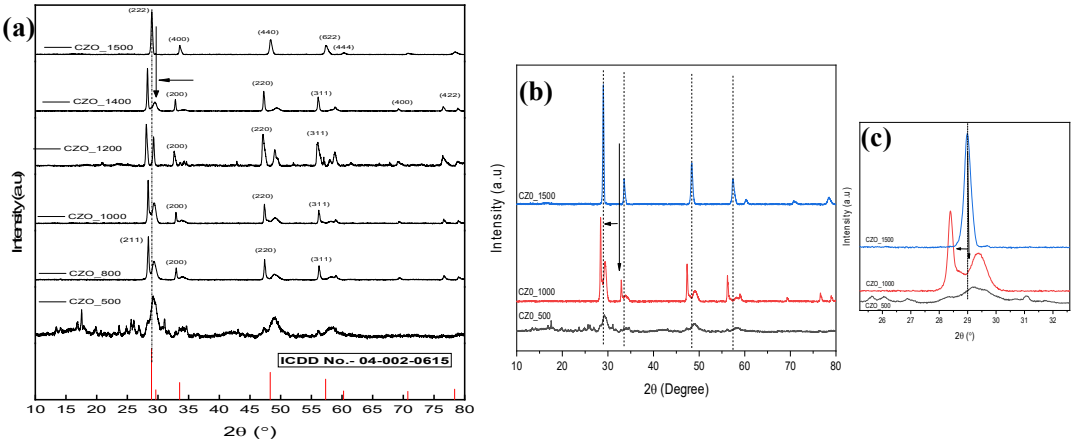

Figure 1: (a) XRD patterns for CZONPs at different annealing temperature of 500^0C, 800^0C,1000^0C, 1200^0C,1400^0C and 1500^0C for 4 hours. (b) and (c) Comparison of selected XRD patterns for CZONPs annealed at 500, 1000, and 1500 °C.

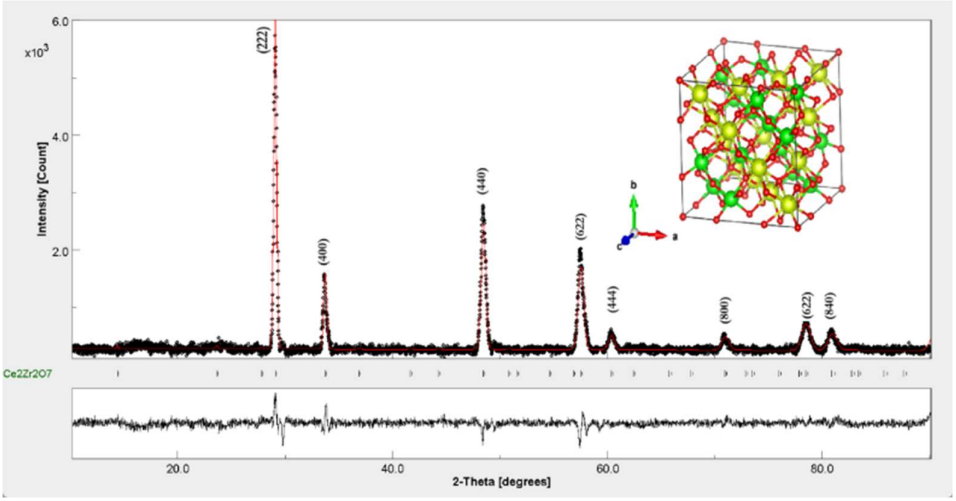

Figure 2: Rietveld refinement of $Ce_2Zr_2O_7$ annealed at 1500 °C. Dots: experimental data; solid line: calculated profile; tick marks: Bragg reflections; bottom line: difference curve.

The average crystallite size of the materials was obtained using Debye Sheerer's equation and William's-Hall fitting was used to determine the strain in the materials.

$$D = \frac{K*\lambda}{\beta cos\theta} \qquad (2)$$

Where β= Full width at half maximum of the selected peaks FWHM, K=0.94 and λ=0.1540nm

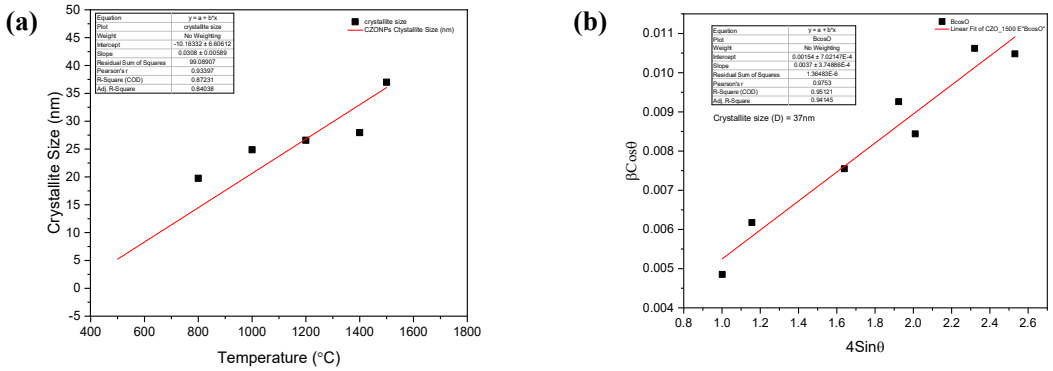

Figure 4: (a)Variation of crystallite sizes with annealing temperature, (b) Williamson–Hall plot for $Ce_2Zr_2O_7$ annealed at 1500 °C.

The calculated values of Crystallite size D(nm), Strain and lattice parameters are shown in Table1 for the respective materials, it can be observed that as the temperature increases, the lattice size also increase from 800 to 1400 and finally decrease at 1500 which change of phase as recrystallization occur, the result obtained is in line with other previous study [6]. The average crystallite size increases with an increase in the annealing temperature which ranges from 19nm to 40nm, this was shown in Figure 4(a). The lattice strain of the materials was obtained using Williamson-Hall fitting Figure 4(b).

$$\beta_T Cos\,\theta = \varepsilon(4Sin\theta) + 4\frac{K\lambda}{D} \qquad (1)$$

β_T = Full width at half maximum of the selected peaks (FWHM), ε = strain, K=0.94, λ =0.1540 nm, the source of X-ray wavelength.

3.2 Morphology analysis

The powder annealed at 500 °C depicted very small isometric particles which are heavily agglomerated. Figure 5 represents the TEM images and SAED patterns of CZONPs annealed at (a) 500°C, (b) 1000 °C, and (c) 1500 °C materials showing particle morphology, as annealing temperature increases to 1000°C the results show cubic and hexagonal and showing improved crystallinity and at an increase temperature of 1500°C is cubic with highly crystalline.

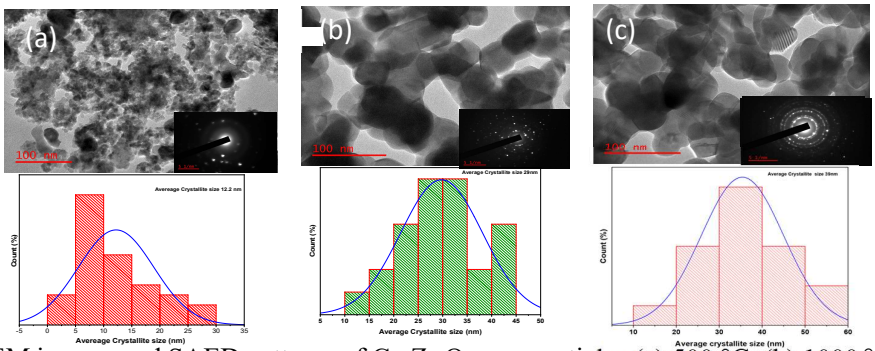

Figure 5. TEM images and SAED patterns of $Ce_2Zr_2O_7$ nanoparticles (a) *500* °C, (b) *1000* °C, and (c) 1500 °C materials showing particle morphology, selected area electron diffraction patterns and normal distribution of materials average crystallite sizes.

3.2 Elemental composition

The elemental formation of was analyzed using EDS. Figure 7 represents SEM micrograph and EDS elemental mapping of $Ce_2Zr_2O_7$ annealed at 1500 °C shows the presence of Ce, Zr and O and $Ce_2Zr_2O_7$ materials contain expected elements and corresponding peaks.

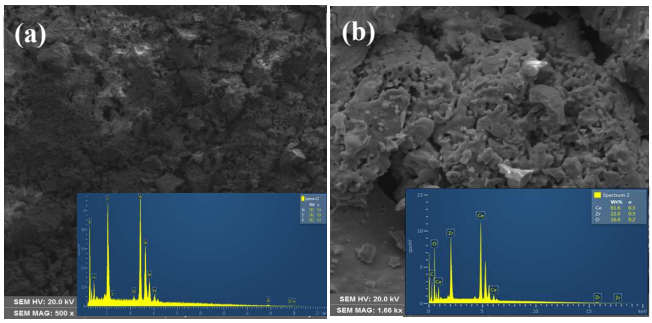

Figure 6: SEM micrograph and EDS elemental of $Ce_2Zr_2O_7$ annealed at (a) 500^0C and (b)1500^0C °C.

The corresponding EDS mapping demonstrates that all cations were present in the analysed powder sample according to its nominal composition. Moreover, the observed elemental distribution showed that elements were randomly and homogeneously distributed throughout the analysed powder sample indicating that the powder chemical homogeneity was achieved due to the selected synthesis procedure. The typical morphology of the obtained compositionally complex oxide powder is shown in Figure 6 (a) and (b), it can be observed that the sample prepared by sol-gel method and annealed at 1500^0C for (4) hours.

Table 1. Rietveld refinements of the X-Ray powder diffraction patterns for CZONPs at different annealing temperature of 500^0C, 800^0C,1000^0C, 1200^0C,1400^0C and 1500^0C for 4 hours

Temperature (^{0}C)	**1500^0C**	**1400^0C**		**1200^0C**		**1000^0C**		**800^0C**	
Rwp	11.2	14.9		13.4		12.8		13.9	
Rexp	5.5	4.5		4.4		4.7		4.6	
GOF	2.0	3.2		3.05		2.73		3.02	
Phase	C- $e_2Zr_2O_7$	C- $Ce_2Zr_2O_8$	t-ZrO_2	C- $Ce_2Zr_2O_8$	t-ZrO_2	C- $Ce_2Zr_2O_8$	t-ZrO_2	C- $Ce_2Zr_2O_8$	t-ZrO_2
Space Group	*Fd-3m*	*P213*	*P21/nmc*	*P213*	*P21/nmc*	*P213*	*P21/nmc*	*P213*	*P21/nmc*
Weight (%)	100	24	76	42	58	55	35	40	60
a (Å)	10.61	10.81	3.67	10.78	3.64	10.75	3.65	10.71	3.69
b ((Å)	10.61	10.81	5.19	10.78	5.53	10.75	5.80	10.71	5.25
c ((Å)	10.61	10.81		10.78		10.75		10.71	
α, β, ϒ	90^0	90^0	90^0	90^0	90^0	90^0	90^0	90^0	90^0
Crystallite Size (nm)	37	27.97		26.85		24.87		19.7	
Strain (x10^{-4})	3.0	3.3		8.6		10.7		23.9	

4. Conclusion.

The $Ce_2Zr_2O_7$ materials were successfully synthesized using the sol-gel method. The study investigated the structure, and morphology of the materials, and found that annealing temperature significantly affects CZONPs. TEM studies reveal the particles morphology which is cubic. The SAED pattern helps confirm the crystallinity and crystallite sizes. The research discovered higher annealing temperatures improve crystallinity, phase purity, reduce strain ($23E^{-4}$ to $3E^{-4}$). Depending on the target application, annealing parameters can be tuned to optimize the material performance. Further research will focus on the optical, thermodynamic, and magnetics properties of the materials.

Acknowledgement
Dr. Mubarak Yagoub and special thanks to University of Johannesburg, URC for the Financial Support.

References

[1] Giampaoli, G., 2018 *Tuning Functional Properties of Pyrochlore and Related Oxides via Cation and Anion Substitutions.*

[2] Muhammad Ashan, Gaber A.M. Mersal, Ahmed Fallatah, M, Ibrahim, Mohamed M, Ahmad, Khurshed, El-Bahy, Zeinhom M. 2005 *Achieving superior supercapacitive performance with rGO-integrated pyrochlore type $Ce_2Zr_2O_7$* Materials Science in Semiconductor *Processing, vol: 185, pg. 108912*

[3] Fuentes, A.F., E.C. O'Quinn, S.M. Montemayor, H. Zhou, M. Lang and R.C. Ewing, 2024 *Pyrochlore-type lanthanide titanates and zirconates: Synthesis, structural peculiarities, and properties.* Applied Physics Reviews. 11(2).

[4] Preuss, A. and R. Gruehn, 1994 *Preparation and structure of cerium titanates Ce2TiO5, Ce_2TiO_7, and $Ce_4Ti_9O_{24}$.* Journal of Solid State Chemistry. 110(2): p. 363-369.

[5] Sardar, S., 2020 *Manufacturing of pyrochlore ($A_2B_2O_7$) nanoparticles using sol gel method*, University of Leeds.

[6] Ashan, M., G.A. Mersal, A.M. Fallatah, M.M. Ibrahim, K. Ahmad and Z.M. El-Bahy, 2025 *Achieving superior supercapacitive performance with rGO-integrated pyrochlore type $Ce_2Zr_2O_7$.* Materials Science in Semiconductor Processing. 185: p. 108912.

[7] Muhammad, P., A. Zada, J. Rashid, S. Hanif, Y. Gao, C. Li, Y. Li, K. Fan and Y. Wang, 2024 *Defect engineering in nanocatalysts: From design and synthesis to applications.* Advanced Functional Materials. 34(29): p. 2314686.

[8] Subramanian, M., G. Aravamudan and G.S. Rao, 1983 *Oxide pyrochlores—a review.* Progress in Solid State Chemistry. 15(2): p. 55-143.

[9] http://maud.radiographema.com

[10] Ahmad Umar, Rajesh Kumar, Girish Kumar, H. Algarni, S.H. Kim**,** 2015 *Effect of annealing temperature on the properties and photocatalytic efficiencies of ZnO nanoparticles,* Journal of Alloys and Compounds, Vol. 648, Pg. 46-52,

[11] Kabekkodu, S. N., Dosen, A. & Blanton, T. N. 2024. Powder Diffr. 39, 47–59.